Enhanced Mechanical Properties of 70/30 Brass Joint by Rapid Cooling Friction Stir Welding

Nan Xu*, Rintaro Ueji and Hidetoshi Fujii

Joining and Welding Research Institute, Osaka University, 11-1 Mihogaoka, Ibaraki, Osaka 567-0047, Japan

Abstract:

The effect of rapid cooling on the microstructure, texture and mechanical properties of friction stir welded 70/30 brass was investigated. Liquid CO_2 was used as the cooling medium during the process. Without the rapid cooling, the welded joint showed many micropores and Zn/Cu oxides in the stir zone accompanied with relatively wide heat affected zone. The stir zone showed a relatively coarse grains with a mean diameter of 9.7 μm and these grain had low dislocation density. The crystallographic texture whose dominant component of {1 0 0} (// shear plane) <0 0 1> (// shear direction) was also found. On the other hand, when the rapid cooling was operated during the welding process, a sound joint with no obvious heat-affect zone was achieved. The stir zone showed the fine grained structure whose mean grain size is 1.2 μm with high dislocation density. The texture in the stir zone was completely different from that in the joint without the rapid cooling. These difference between the joints with and without the rapid cooling indicates the significant post annealing effect including both recovery and static recrystallization can be prohibited by the rapid cooling. As a result, the enhanced the yield strength with adequate ductility of the stir zone was obtained.

Keywords: 70/30 brass; Rapid cooling FSW; Microstructure; Texture; Mechanical properties

* Corresponding author: Tel./fax: +81 06 6879 8663; E-mail: xu@jwri.osaka-u.ac.jp; xunan20032389@126.com (Nan Xu).

1. Introduction

70/30 Brass offers very useful properties, such as a high strength, thermal and electrical conductivities, plastic formability and corrosion resistance, thus it is widely used in industrial applications **[1]**. The joining of 70/30 brass is very difficult by conventional fusion welding because the 70/30 brass has a high thermal diffusivity, which is about 10-100 times higher than in steels and nickel alloys **[2]**, therefore, a large heat input is required. However, the large heat input causes evaporation of the Zn, resulting in large pores being produced in the fusion zone **[3]**, which remarkably reduces the mechanical properties of the joint.

While these problems have not been totally solved for fusion welding, it seems that friction stir welding (FSW, abbreviations of technical terms used in the present paper were listed in **Table 1**), which is a solid-state joining technique invented by The Welding Institute (TWI) in 1991 **[4]**, is a very useful method for the joining of various kinds of metals. For FSW, two plates are clamped and butt-welded by plunging a high-speed rotating tool into the interface of the plates and moving it along the weld center. During the FSW process, the frictional forces between the tool and plates create intense local heating that does not melt the plates, but softens the material. The rotating tool causes material transfer around the tool, thus stirring the plates to be joined. In the past two decades, several researches have encompassed a wide range of structural materials including hexagonal close packed, body-centered cubic and face-centered cubic with different stacking fault energies **[5]**. However, comparatively little attention has been given to this process for 70/30 brass which is a kind of face-centered cubic alloy with an extremely low stacking fault energy. Meran **[6]** initially introduced FSW to the joining of 70/30 brass, and pointed out that the evaporation of Zn and the formation of pores were completely prevented. The strength of the obtained stir zone (SZ) can

approach that of the base metal (BM) level, but the fracture occurred in the heat-affected zone (HAZ) where grain coarsening appeared. After that, few investigations about the FSW of 70/30 brass were undertaken **[7,8]**. Moghaddam et al. **[7]** studied the FSW of the 70/30 brass at various welding speeds and found that a "stir band", which is comprised of micro-porosities and copper/zinc oxidation, formed in the SZ. Sun et al. **[8]** studied the FSW of the 70/30 brass under various welding conditions, and found that a zigzag black line, which is composed of a distribution of oxide particles formed in the SZ. Although the micro-porosities and oxide particles do not influence the strength of the SZ **[7,8]**, they significantly reduce the ductility for the increasing stress concentration during the tensile test **[7]**.

The number of papers reporting the microstructure generated in the FSW joint of the 70/30 brass is also limited. Sun et al. **[8]** reported that their transmission electronic microscopy (TEM) observations clarified the formation of dislocation cells in the SZ of the 70/30 brass joint. As is well known, the cell structure can develop by recovery **[9]**. However, recovery hardly occurs in face-centered cubic metals with a low stacking fault energy. On the other hand, the stacking fault energy increases with the increasing temperature **[10]**. Therefore, even though the 70/30 brass has a low stacking fault energy at ambient temperature, the reconstruction of the dislocation arrangements by recovery can take place during the stirring or the post stage of stirring at which the sample is at a high temperature. The reconstruction by recovery is important for industrial applications since it has a significant effect on the strength of the materials. In order to control the recovery and related annealing phenomena, it should be useful to examine the microstructure of the FSW joint with rapid cooling which can remove the post-annealing effect.

Based on the above mentioned results, the following two aspects can be achieved. First, the

common FSW needs a larger heat input which leads to the oxidation and microporosities which should be removed. Second, the SZ shows an annealed structure with few substructures due to the post-annealing effect. Therefore, in this study, rapid cooling FSW (RC-FSW) was developed during the welding process, and the aim was to obtain a defect-free 70/30 brass joint without the HAZ and provide the possibility of microstructure control for further strengthening.

2. Experiments

Cold-rolled commercial 70/30 brass plates of 1/4H condition with dimensions of $140^{L} \times 70^{W} \times 2^{T}$ mm were used in this study. The chemical composition of the alloy is 69.5 % Cu, 0.004 % Pb, 0.001 % Fe and Zn as balance. The welding conditions and tool dimensions used in this study are summarized in **Table 2**. The rotating tool was made of a WC based material and equipped with a columnar probe with no thread. Rapid cooling was attained by directing liquid CO_2 toward the weld centerline during the welding through two nozzles set at 5 cm back from the FSW tool **[11,12]**.

After the FSW, the samples were cross-sectioned perpendicular to the welding direction, polished and then etched with a solution of 2.5 g iron (Ⅲ) chloride, 100 ml distilled water and 15 ml hydrochloric acid for the optical microscopy observations. An energy dispersive X-ray spectrometer (EDS) attached to a JEM-7001FA field-emission scanning electron microscope (FE-SEM) was used for the elemental analysis. An electron backscattered diffraction (EBSD) measurement was conducted in the central SZ using a TSL OIM ^{TM} system which was also attached to the FE-SEM. The step size of the EBSD scanning was 0.2 μm. The substructures in the central SZ were characterized by a JEM-2100F TEM. For the TEM sample preparation, thin polished samples were double-jet electro-polished using a solution of HPO_4:CH_4O:H_2O=1:1:2 in volume at 5 V and -30 °C. For the tensile tests, the transverse tensile specimens covering various regions with a gauge size of

$28^{L} \times 5^{W} \times 1.8^{T}$ mm^3 were machined with the tensile axis perpendicular to the welding direction. The specimens containing only the SZ were also machined with a gauge size of $12^{L} \times 3^{W} \times 1.8^{T}$ mm^3 and the tensile axis parallel to the welding direction to evaluate the tensile strength of the SZ. The tensile tests were carried out using an Instron-type testing machine at a crosshead speed of 1 mm/min at room temperature.

3. Results and discussion

3.1 Microstructure evolution and texture development

Optical microscopy images of the cross-section of the common-FSW and RC-FSW 70/30 brass joints are shown in the top of **Fig. 1**. A basin-shaped SZ widens from the bottom to the top surface can be observed in both of the joints. This morphology was frequently found in the FSW joints of pure copper and its alloy, and it was postulated to be caused by the friction between the work-piece surface and the shoulder of the rotation tools **[8,13]**. The enlarged images of the microstructures at the transition zones of AS indicated by the black rectangle in the top images are shown at the bottom of **Fig.1**. For the common-FSW joint, the transition zone exhibits an HAZ with its mean grain size (46.7 μm) larger than that of the BM (31.5 μm) and the thermo-mechanically affected zone (TMAZ) with its elongated grains aligned in the material flow direction. The grains in the TMAZ are occasionally elongated with the mean ratio aspect of 2.8. This is mainly due to shear deformation. These morphologies were widely reported in previous FSW researches about copper and its alloy **[8,13-15]**. For the RC-FSW joint, however, the average grain size outside the BM/TMAZ boundary line was 32.1 μm which is similar to that of the BM. On the other hand, the TMAZ of the RC-FSW joint mainly consisted of fine grains whose grain size is similar to the SZ. Additionally, some of the elongated grains can also be observed but their number is limited. This was caused by the rapid

thermal dissipation.

SEM images of the SZs of the common-FSW and RC-FSW joints are shown in **Fig. 2.** For the SZ of the common-FSW joint, many micro-porosities and particles were detected (**Fig. 2a**). These defects were preferentially observed in the area near the top surface. An EDS point analysis performed on one of theses particles mainly revealed the presence of copper and zinc elements. A trace amount of oxygen was also detected which can be attributed to oxide formations (**Fig. 3**). Since the SZ experienced a relatively high temperature **[16]**, Zn/Cu oxides easily appeared and separated by the stirring, resulting in a significant number of pores and oxide. Formation of the porosities and particles has already been reported as a typical phenomenon in the FSW of 70/30 brass **[7,8,16]**. On the other hand, a sound FSW joint without any oxides and porosities can be obtained since the SZ of the RC-FSW joint underwent a relatively low peak temperature and fast cooling rate by the rapid cooling **[16]** (**Fig. 2b**).

The EBSD measurements were examined on the central SZ of the two joints as well as the BM. The obtained results including the grain boundary maps and the misorientation angle distributions are shown in **Fig. 4** and **Fig. 5**, respectively. The BM has a large quantity of twin boundaries and low angle boundaries due to the BM that was produced by the annealing and subsequent cold-rolling (1/4H condition). The SZ of the common-FSW joint was characterized by recrystallized grains, and the average grain size was determined to be 9.7 μm. The grain boundary map reveals a high fraction of high angle boundaries (94.3 %) and approximately 35.9 % of the high angle boundaries were classified as twin boundaries, while the number fraction of the low angle boundaries was only 5.7 %. This fraction is slightly higher than that calculated based on the assumption of randomly aligned grains (dotted line) **[17]**. For the RC-FSW joint, on the other hand, the SZ shows uniform ultrafined

grains with its mean grain size of 1.2 μm, and the number fraction of the low angle boundaries was up to 36.2 %. The differences between the common-FSW and the RC-FSW joints clearly indicate that the post-annealing effect provides both the recovery (low angle boundaries) and static recrystallization (high angle boundaries).

The 0 0 1, 0 1 1 and 1 1 1 pore figures of the SZ of the common-FSW and RC-FSW joints, as well as the BM, are shown in **Fig. 6**. The BM exhibited a relatively random texture due to the low stacking fault energy **[9]**. It is interesting that the SZs of the common-FSW joint and RC-FSW joint showed different textures. For the RC-FSW joint, the texture at the center of the SZ predominantly consists of the {-1 1 2}<1 1 0> component in which the rotation tangent (TD) and radius (WD) directions were <1 1 0> and <-1 1 2>, respectively. This component can be categorized as the type B shear texture according to the assumption for the plastic shear flow that the rotation tangent and the radius directions are parallel to the shear direction and the shear plane normal **[18]**. The strongest concentration of the orientation is placed at the TD//[0 1 1] and the broad tendency of rotation around the TD to form a fiber character is found. This character has a good agreement with the fact that <0 1 1> is the preferable orientation for the shear direction in the face-centered cubic metals monotonically formed by the shear deformation **[18]**. This kind of shear texture is usually observed in the SZ near the probe of the friction stir processed face-centered cubic metals or alloys such as 1050 aluminum alloy **[19]** and 4N-Cu **[20]**.

In contrast, the SZ of the common-FSW mainly exhibited a {1 0 0} <0 0 1> orientation (**Fig. 6**). When WD and TD are regarded to analogically act in the same manners as the rolling direction and normal direction in a rolling sheet, {1 0 0}<0 0 1> can be considered as a kind of cube orientation which is a static recrystallization texture frequently observed in 70/30 brass **[9]**. It should be noted

that the {-1 1 2}<1 1 0> orientation still remained, but the intensity was remarkably weakened. It is likely that the post-annealing effect lead to the texture transformation from the {-1 1 2}<1 1 0> to {1 0 0} <0 0 1> orientation. This change in texture means that the post-annealing provides a significant opportunity for static recrystallization. The recrystallization is a long range movement of the boundaries newly introduced by plastic deformation and the driving force of the movement is the difference in the stored energy of the adjacent areas such as the difference in the dislocation density. The dislocation density changes during the plastic deformation with a strong dependence of the crystallographic orientation. For example, the regions with a cube orientation in the rolled sheet are difficult to obtain a high density of stored dislocations due to the crystallographic symmetry **[9]**. The lack of dislocation enhances the selected grain growth so that cube orientation becomes dominant after the recrystallization. As indicated by the relatively simple texture of RC-FSW, the effect of plastic deformation by FSW on the texture is considered as the same manner as the simple monotonic deformation. Therefore, it is not doubtful that the simple texture component evolves in the FSW joint after adequate annealing.

TEM images of the SZs obtained with/without rapid cooling are shown in **Fig. 7**. Large annealing twin boundaries with few dislocations were observed in the SZ of the common-FSW joint (**Fig. 7a**). However, ultrafine grains with a high dislocation density were detected in the SZ of the RC-FSW joint (**Fig. 7b**). The TEM images suggest that the low angle boundaries in the grain boundary map are associated with the dislocation density, and the TEM results well matched the EBSD measurements. It is well-known that recrystallization and plastic deformation cause grain refinement and dislocation generation during the FSW **[8,12,13,20-22]**. Based on the EBSD results and TEM observations, it is concluded that the shear texture and ultrafine grains with a high dislocation density,

which were generated around the rotating tool, was maintained in the SZ after the tool passed through for prevention of the post-annealing effect.

3.2 Mechanical properties

Fig. 8 shows the Vickers hardness of the joints obtained under the different cooling conditions. The BM exhibited relatively high hardness values of 105-108 Hv due to the initial work hardened state. The common-FSW joint exhibited a reduced hardness throughout the weld region, which is attributed to the grain coarsening caused by the annealing **[15,23,24]**. A wide low-hardness zone was clearly observed in the HAZ, with a lowest hardness value of about 91 Hv. Moreover, although the grain size in the SZ was refined, the hardness profiles were still lower than that of the BM due to disappearance of the substructures caused by the post-annealing effect. Similar results were reported by Hwang et al. **[23]** and Lee et al. **[25]**, who also found that the hardness of the SZ of the FSWed copper joints was lower than that of the BM. However, for the RC-FSW joint, no low-hardness zone was observed, and the hardness of the SZ was much higher than that of the BM due to the ultrafine grained structure and the large number fraction of low angle boundaries which were mainly composed of dislocation cells.

Tensile tests were carried out to evaluate the mechanical properties of the joints obtained with/without rapid cooling. For the global tensile specimen containing the BM and welded joint, the common-FSW specimen fractured at the HAZ in the low-hardness zone located in that region (**Fig. 9a**). It is widely accepted that the HAZ is the softest zone and determines the mechanical properties of the entire FSWed joints **[15,24-26]**. However, the RC-FSW specimen fractured at the BM, indicating the increased tensile strength of the welded joint due to the totally absent low-hardness

zone and the strengthened SZ (**Fig. 9b**). In order to evaluate the exact tensile strength of the SZ, miniature tensile tests of the SZ were carried out, and the obtained engineering stress-strain curves are shown in **Fig. 10**. The SZ of the common-FSW joint shows the lowest yield strength of 183 MPa for the SZ having an annealed structure with a low dislocation density caused by the post effect. As we know, during the work hardening stage, the start of necking in tension is governed by the Considère's criterion as follows:

$$\frac{d\sigma}{d\varepsilon} \leq \sigma \tag{1}$$

This equation means that the elongation significantly depends on the work hardening behavior when the specimen has a sufficient capacity of plastic deformation. However, during the early stage of the tensile test up to around 17 %, the difference in the work hardening rate between the common-FSW and the BM is not very obvious, indicating that the common-FSW breaks without necking. This means that the common-FSW contains nuclei for fracture which provides no effect on the plastic deformation. The cavity as shown in **Fig. 3** should be one of the nuclei for the fracture. As a result, it exhibited the relatively low ultimate tensile strength of 254 MPa. On the other hand, the SZ of the RC-FSW joint exhibited an enhanced yield strength of 304 MPa, much higher than that of other researches about FSW 70/30 brass **[6-8]** as well as the BM used in this study. The enhanced yield strength resulted from the ultrafine grains with a high dislocation density in the SZ. The SZ of RC-FSW has no cavity so that it was fractured with necking, and the relatively high ultimate tensile strength of 498 MPa obtained. In addition, an elongation of 26 % was also achieved due to the large quantity of twin boundaries in the SZ. The presence of abundant twin boundaries created more local sites for nucleating and accommodating dislocations, thereby elevating the strain hardening during the tensile test **[27-29]**. Above all, the RC-FSW joint shows excellent tensile properties due to both

the success of dislocation storage and the prevention of cavity formation.

4. Conclusions

In this study, the effect of rapid cooling on the microstructure, texture and mechanical properties of friction stir welded 70/30 brass was investigated. The main conclusions are summarized below:

(1) Without rapid cooling, the welded joint showed a relatively wide HAZ, and many micropores and Zn/Cu oxides were generated in the SZ. Liquid CO_2 rapid cooling can improve the thermal cycle during the FSW and produce a weld joint with no obvious HAZ and defect-free SZ.

(2) The post-annealing effect after the FSW process lead to the disappearance of dislocations and grain coarsening in the SZ, and also made the {-1 1 2}<1 1 0> shear orientation transform to the {1 0 0} <0 0 1> recrystallization orientation. In contrast, liquid CO_2 cooling can significantly reduce the post-annealing effect, resulting in the shear orientation and ultrafine grains with a high dislocation density, which were caused by the rotating tool, were maintained in the SZ.

(3) Based on the tensile tests results, the common-FSW fractured in the low-hardness zone which was located at the HAZ, and the SZ exhibited a relatively low strength and ductility due to the existence of cavities and Zn/Cu oxides in the SZ. However, for the RC-FSW joint, the yield strength of the SZ was enhanced to 304 MPa, and the low-hardness zone disappeared, resulting in the fracture occurring in the BM, and the SZ showed excellent elongation and ultimate tensile strength due to both the success of the dislocation storage and the prevention of cavity formation.

Acknowledgements

The authors are thankful for the financial support of the project for heterostructure control from the Japan Science and Technology Agency (JST), the Priority Assistance for the Formation of Worldwide Renowned Centers of Research – The Global COE Program (Project: Center of Excellence for Advanced Structural and Functional Materials Design) and the Cooperative Research Project of Nationwide Joint from the Ministry of Education, Culture, Sports, Science and Technology (MEXT), Japan, and a Grant-in-Aid for Science Research from the Japan Society for Promotion of Science.

References

[1] S. Pasebani, M.R. Toroghinejad, M. Hosseini, J. Szpunar, Mater. Sci. Eng. A 527 (2010) 2050-2056.

[2] E. Biro, D.C. Weckman, Y. Zhou, Metall. Mater. Trans. A 33 (2002) 2019-2030.

[3] C. Meran, M. Yuksel, A. Gulsoz, T. Sekercioglu, Sci. Technol. Weld. Joining 9 (2004) 131-137.

[4] R.S. Mishra, Z.Y. Ma, Mater. Sci. Eng. R, 50 (2005) 1-78.

[5] S. Mironov, Y.S. Sato, H. Kokawa, H. Inoue, S. Tsuge, Acta Mater. 59 (2011) 5472-5481.

[6] C. Meran, Mater. Des. 27 (2006) 719-726.

[7] M.S. Moghaddam, R. Parvizi, M.H. Sabzevar, A. Davoodi, Mater. Des. 32 (2011) 2749-2755.

[8] Y.F. Sun, N. Xu, H. Fujii, Mater. Sci. Eng. A 589 (2014) 228-234.

[9] F.J. Humphreys, M. Hatherly, Recrystallization and related annealing phenomena (2nd ed.), (2004), Elsevier.

[10] S.E. Bühler, K. Lücke, F.W. Rosenbaum, Phys. Stat. Sol. 3 (1963) 886-900.

[11] H. Fujii, Y.D. Chung, Y. F. Sun, Sci. Technol. Weld. Joining 18 (2013) 500-506.

[12] N. Xu, R. Ueji, Y. Morisada, H. Fujii, Mater. Des. 56 (2014) 20-25.

[13] Y. F. Sun, H. Fujii, Mater. Sci. Eng. A 527 (2010) 6879-6886.

[14] H.J. Liu, J.J. Shen, Y.X. Huang, L.Y. Kuang, C. Liu, C. Li, Sci. Technol. Weld. Joining 14 (2009) 577-583.

[15] P. Xue, G.M. Xie, B.L. Xiao, Z.Y. Ma, L. Geng, Metall. Mater. Trans. A 41 (2010) 2010-2021.

[16] N. Xu, R. Ueji, Y. Morisada, H. Fujii, in: H. Fujii (Eds.), Proceedings of the 1st International Joint Symposium on Joining and Welding, Woodhead publishing, Inc. Cambridge, 2013, pp. 169-172.

[17] J.K. Mackenzie, Biometrika 45 (1958), 229-240.

[18] R.W. Fonda, K.E. Knipling, Sci. Technol. Weld. Joining 16 (2011) 288-294.

[19] S. Mironov, K. Masaki, Y.S. Sato, H. Kokawa, Metall. Mater. Trans. A 44 (2013) 1153-1157.

[20] J.Q. Su, T.W. Nelson, T.R. McNelley, R.S. Mishra, Mater. Sci. Eng. A 528 (2011) 5458-5464.

[21] P. Xue, B.L. Xiao, Z.Y. Ma, Mater. Sci. Eng. A 532 (2012) 106-110.

[22] Y.F Sun, H. Fujii, Y. Takada, N. Tsuji, K. Nakata, K. Nogi, Mater. Sci. Eng. A 527 (2009) 317-321.

[23] Y.M. Hwang, P.L. Fan, C.H. Lin, J. Mater. Process. Technol. 210 (2010) 1667-1672.

[24] P. Xue, B.L. Xiao, Q. Zhang, Z.Y. Ma, Scripta Mater 64 (2011) 1051-1054.

[25] W.B. Lee, S.B. Jung, Mater. Lett. 58 (2004) 1041-1046.

[26] H.J. Liu, H. Fujii, M. Maeda, K. Nogi, J. Mater. Proc. Tech. 142 (2003) 692-696.

[27] L. Lu, Y. Shen, X. Chen, L. Qian, K. Lu, Science 304 (2004) 422-426.

[28] K. Lu, L. Lu, S. Suresh, Science 324 (2009) 349-352.

[29] Z.S. You, L. Lu, K.Lu, Acta Mater. 59 (2011) 6927-6937.

Tables list

Table 1 Abbreviations of the technical terms used in this paper.

Technical terms	Abbreviations
Friction stir welding	FSW
Stir zone	SZ
Base metal	BM
Heat-affected zone	HAZ
Transmission electron microscopy	TEM
Rapid cooling friction stir welding	RC-FSW
Energy dispersive X-ray spectrometer	EDS
Field-emission scanning electron microscope	FE-SEM
Electron backscattered diffraction	EBSD
Transverse direction	TD
Normal direction	ND
Welding direction	WD
Advancing side	AS
Retreating side	RS
Thermo-mechanically affected zone	TMAZ

Table 2 FSW conditions and tool size used in this study.

Welding conditions					
Label	Rotation rate (rpm)	Welding speed (mm/min)	Load (t)	Tile angle (deg.)	Cooling media
common-FSW	600	200	1.5	3	Air
RC-FSW	600	200	1.5	3	Liquid CO_2
Tool size					
Shoulder diameter (mm)		Probe diameter (mm)		Probe length (mm)	
12		4		1.9	

Figures List

Figure 1

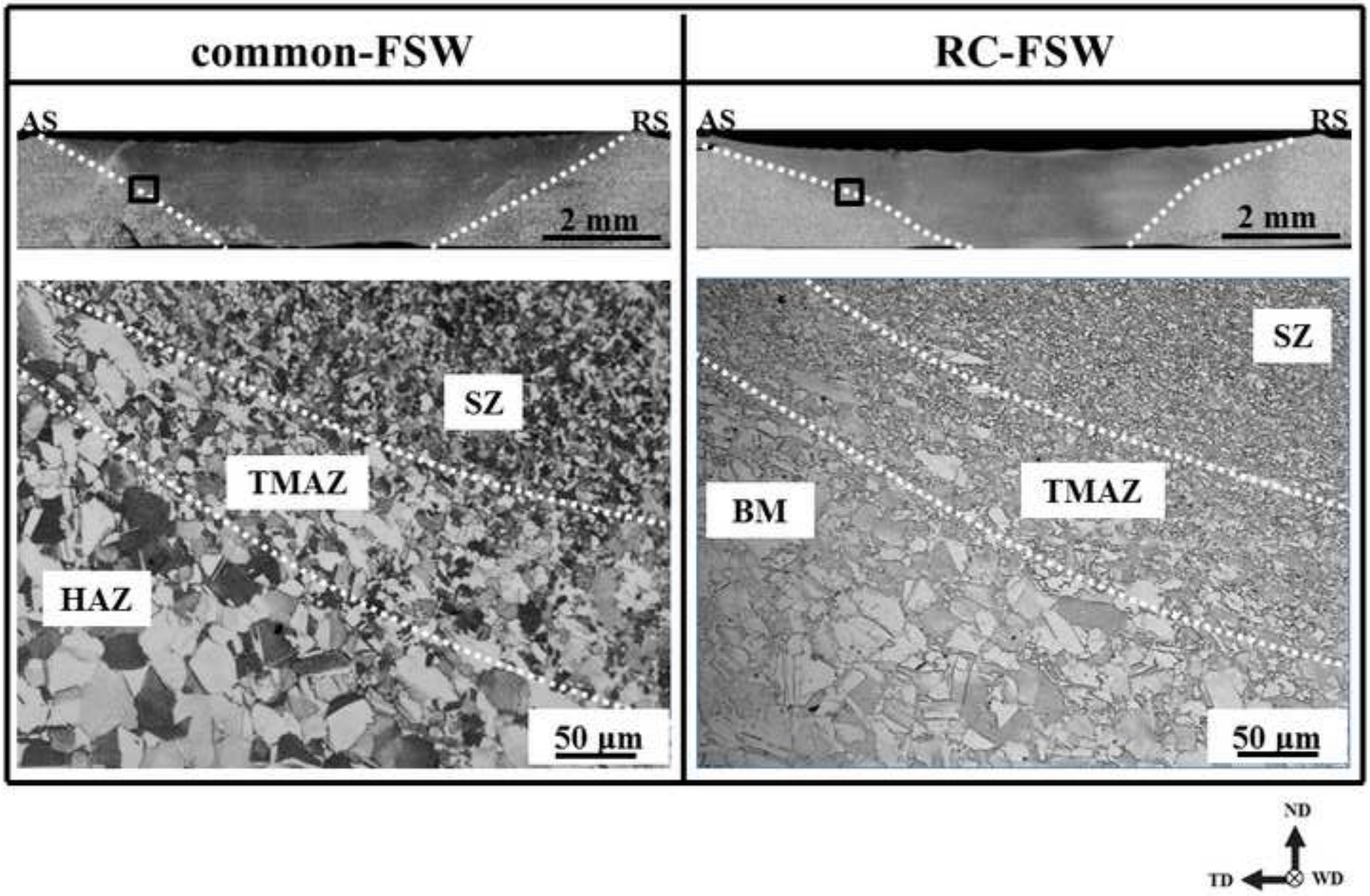

Figure 2

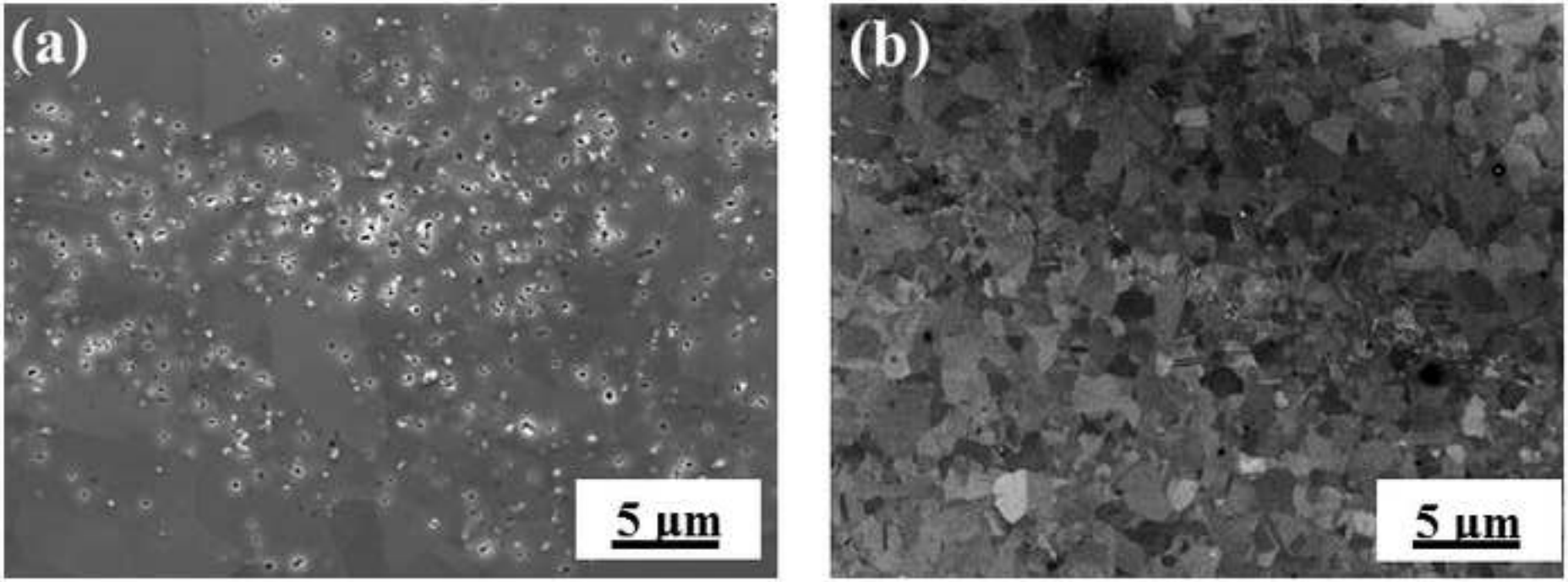

Figure 3

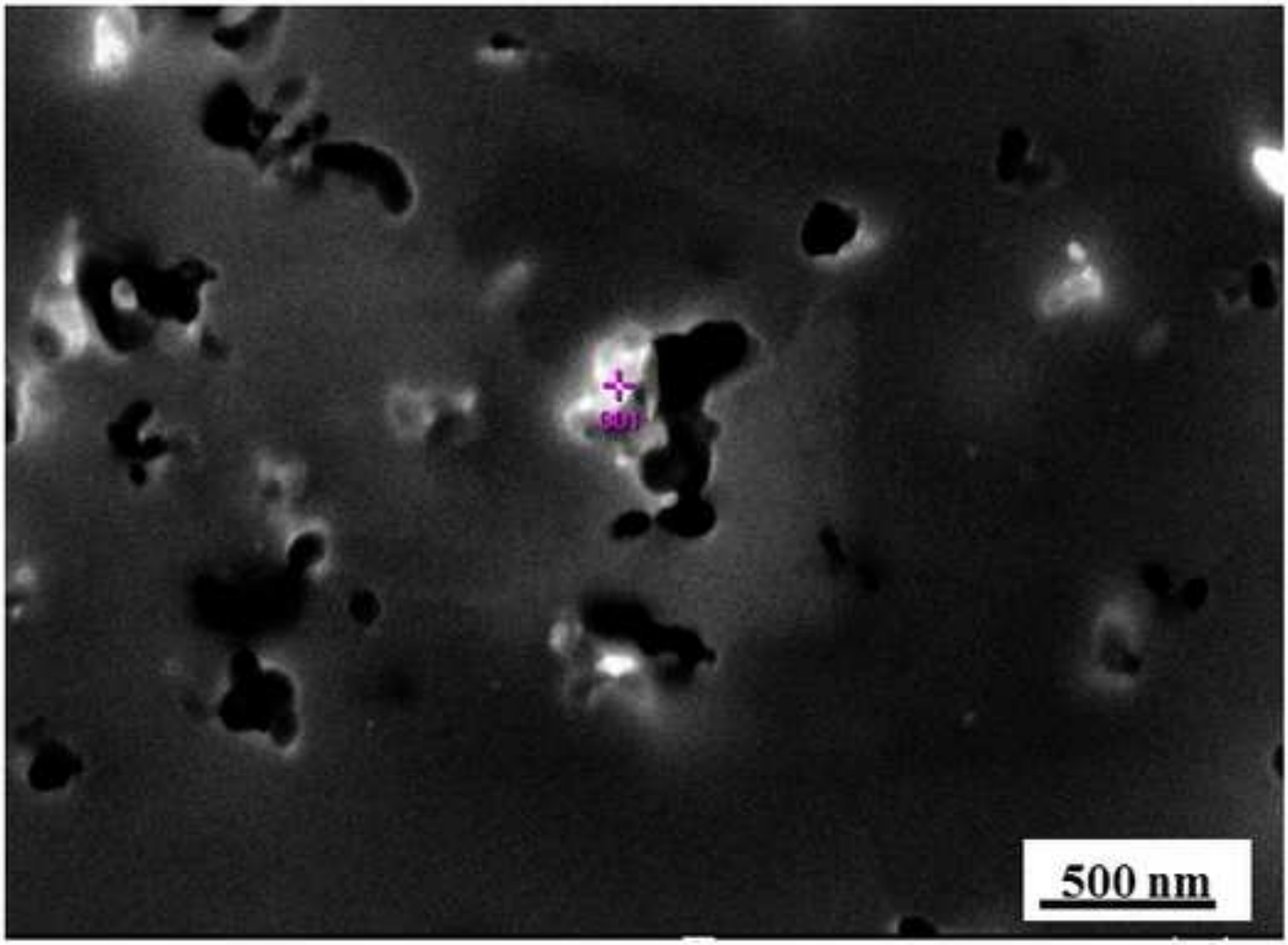
500 nm

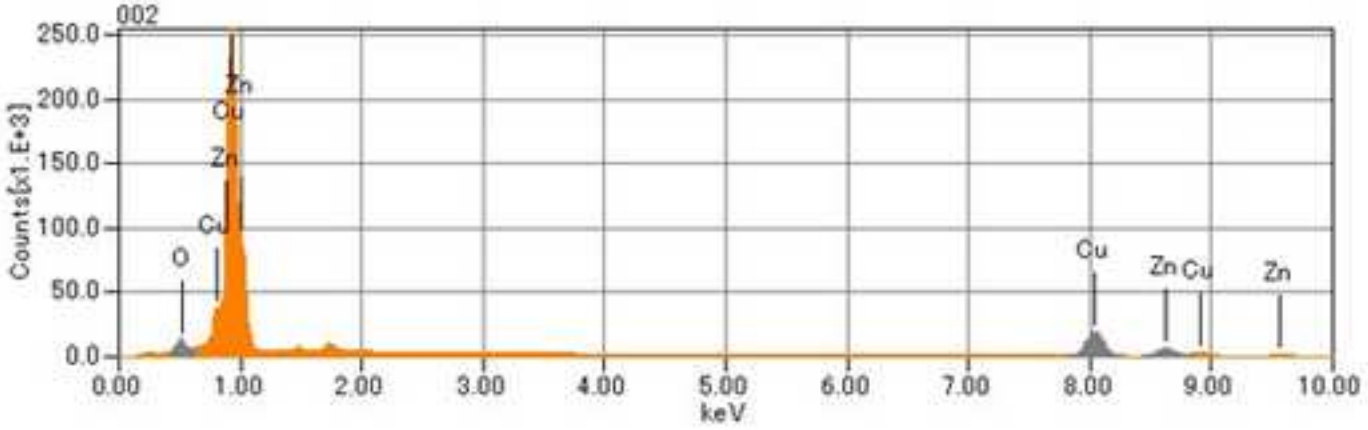
002
250.0
200.0
150.0
100.0
50.0
0.0
Counts[x1.E+3]
O
Cu
Zn
Cu
Zn
Cu
Zn Cu
Zn
0.00
1.00
2.00
3.00
4.00
5.00
6.00
7.00
8.00
9.00
10.00
keV

Figure 4

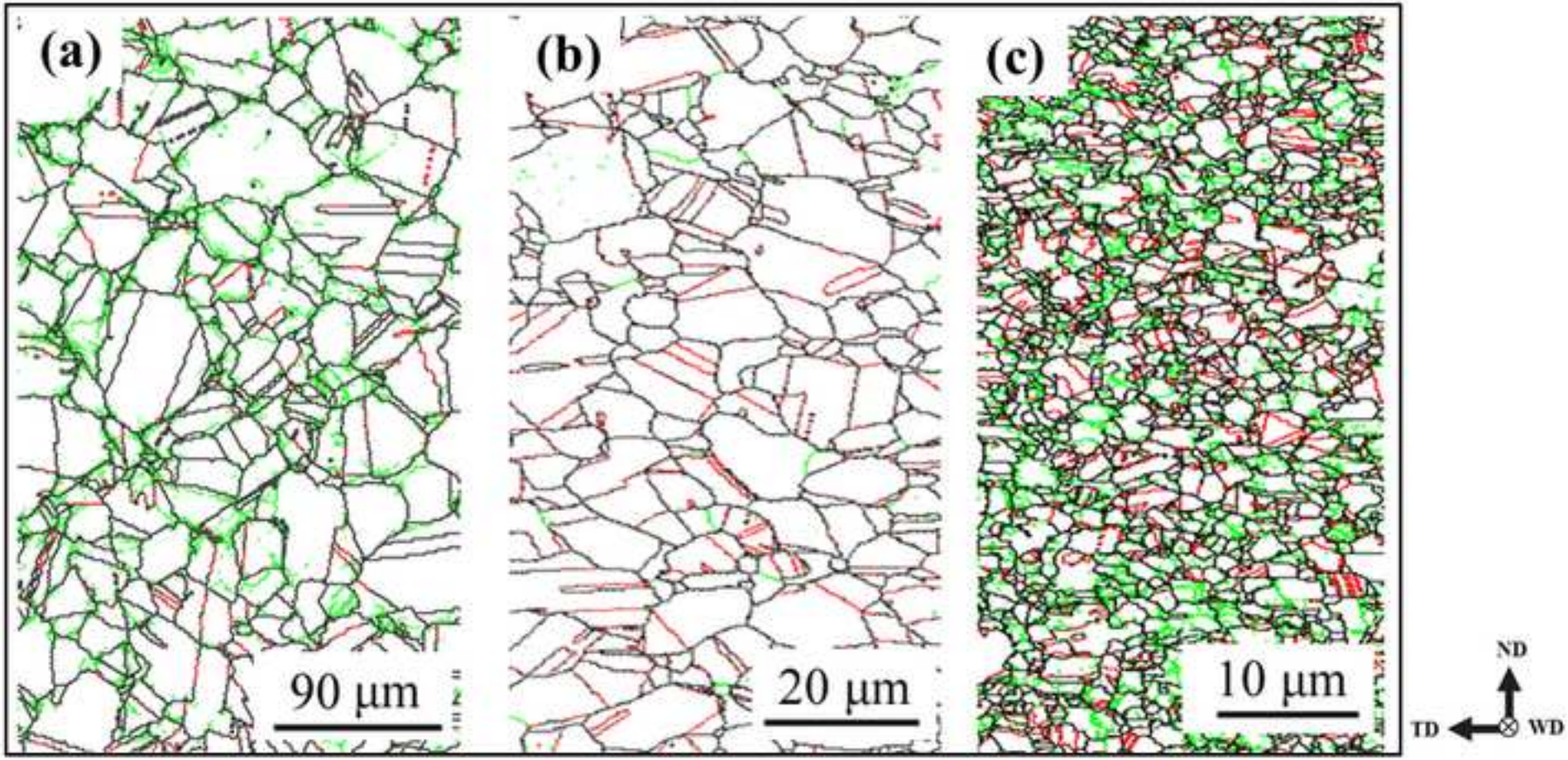

Figure 5

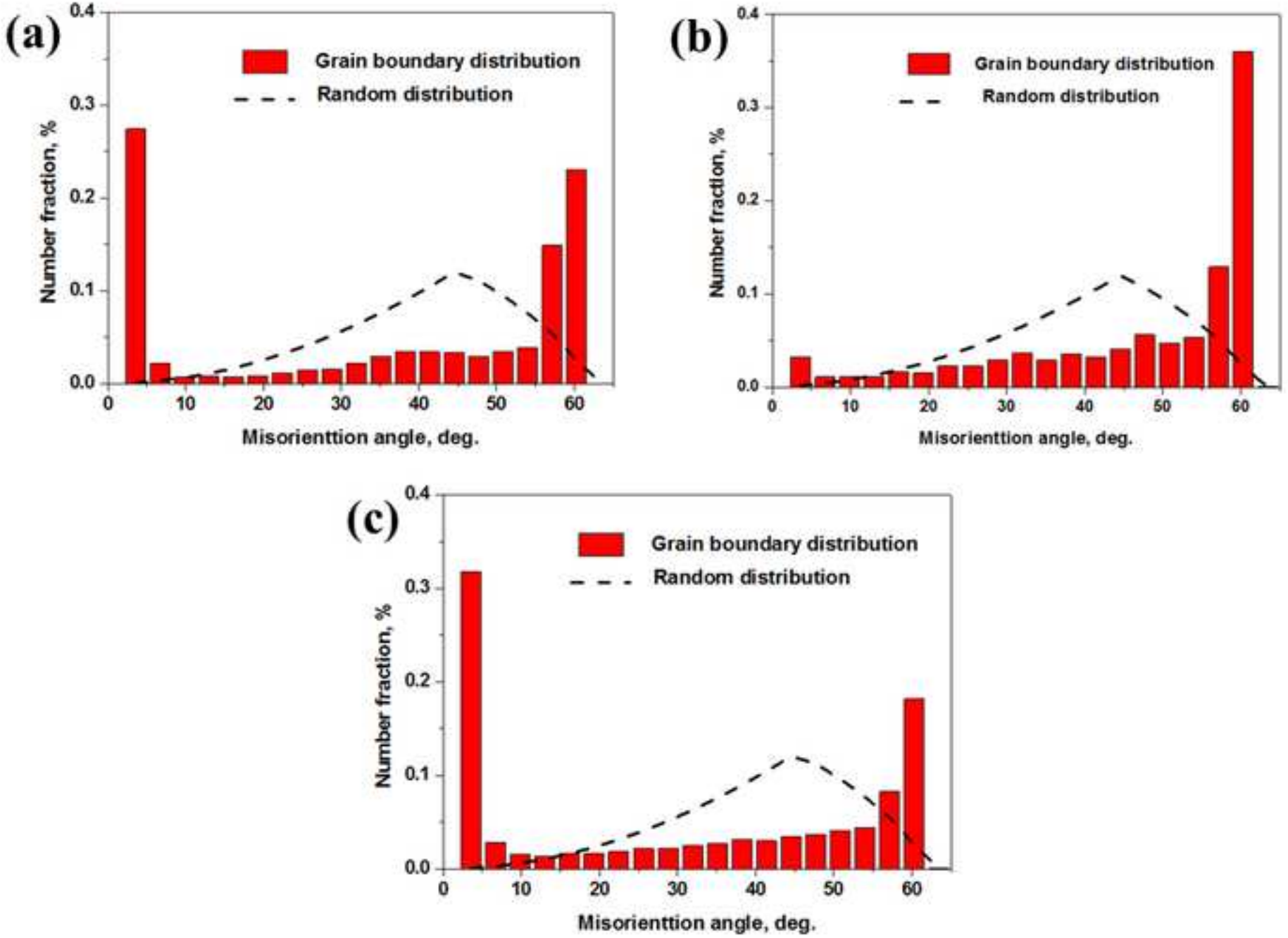
(a)
Grain boundary distribution
Random distribution
Number fraction, %
Misorienttion angle, deg.
(b)
Grain boundary distribution
Random distribution
Number fraction, %
Misorienttion angle, deg.
(c)
Grain boundary distribution
Random distribution
Number fraction, %
Misorienttion angle, deg.

Figure 6

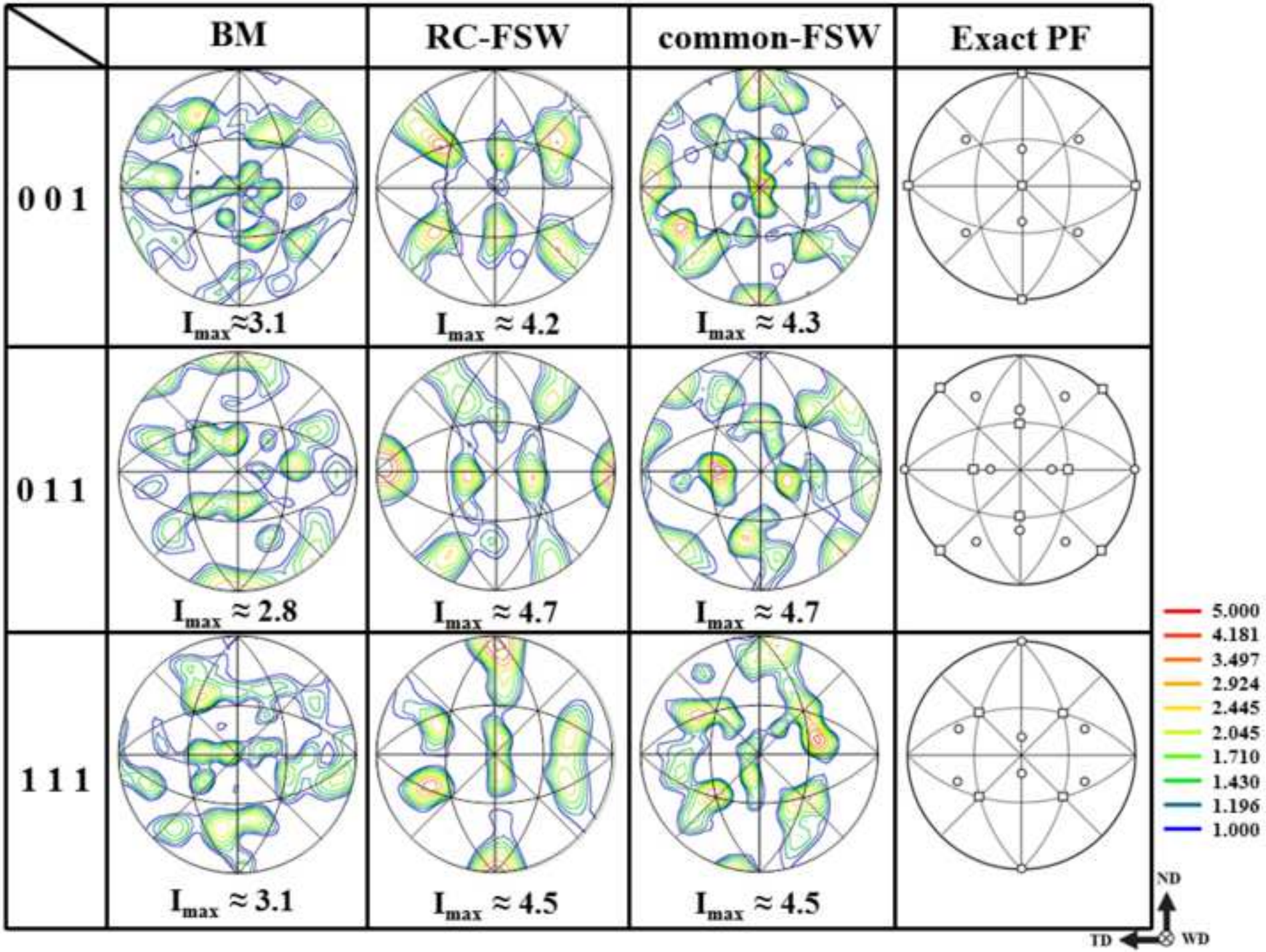
BM
RC-FSW
common-FSW
Exact PF
0 0 1
0 1 1
1 1 1
I_{max}≈3.1
I_{max} ≈ 4.2
I_{max} ≈ 4.3
I_{max} ≈ 2.8
I_{max} ≈ 4.7
I_{max} ≈ 4.7
I_{max} ≈ 3.1
I_{max} ≈ 4.5
I_{max} ≈ 4.5
5.000
4.181
3.497
2.924
2.445
2.045
1.710
1.430
1.196
1.000
ND
TD
WD

Figure 7

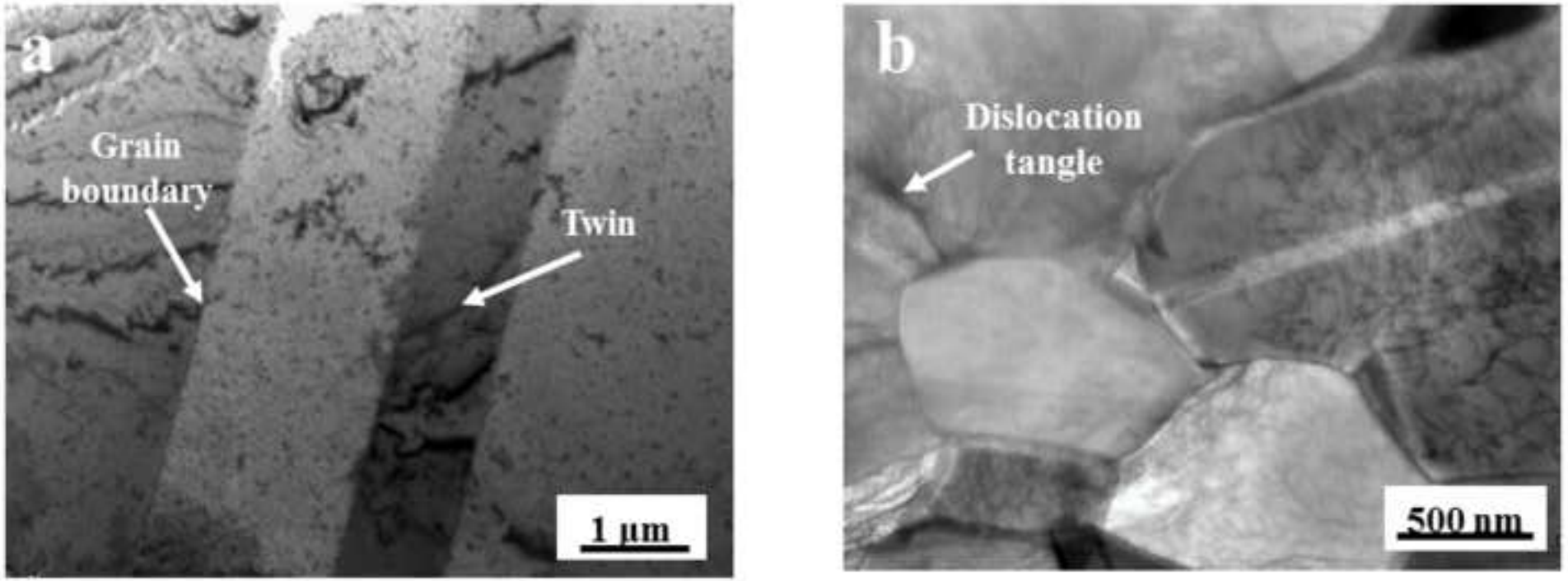

Figure 8

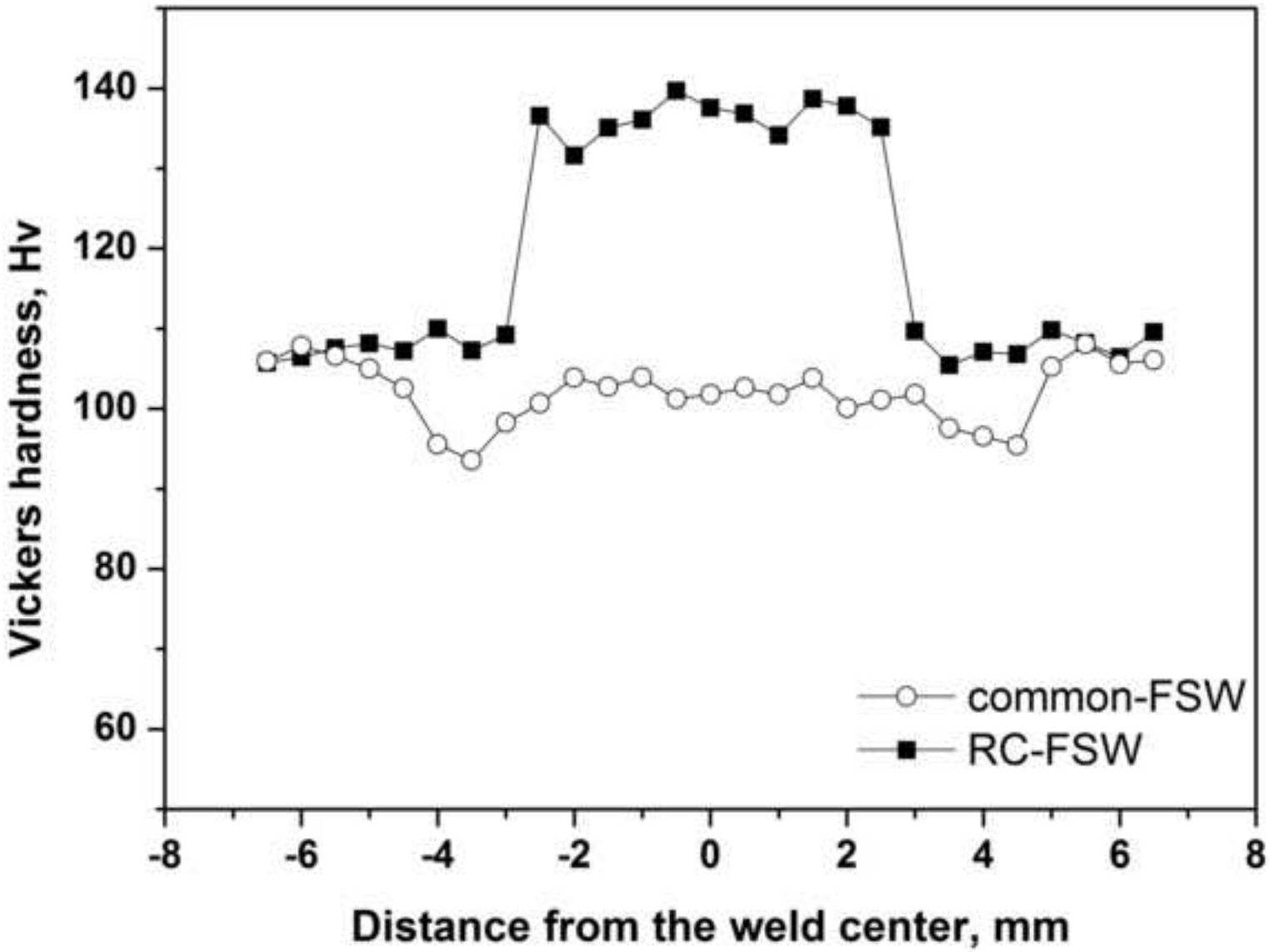
Vickers hardness, Hv
140
120
100
80
60
-8
-6
-4
-2
0
2
4
6
8
Distance from the weld center, mm
common-FSW
RC-FSW

Figure 9

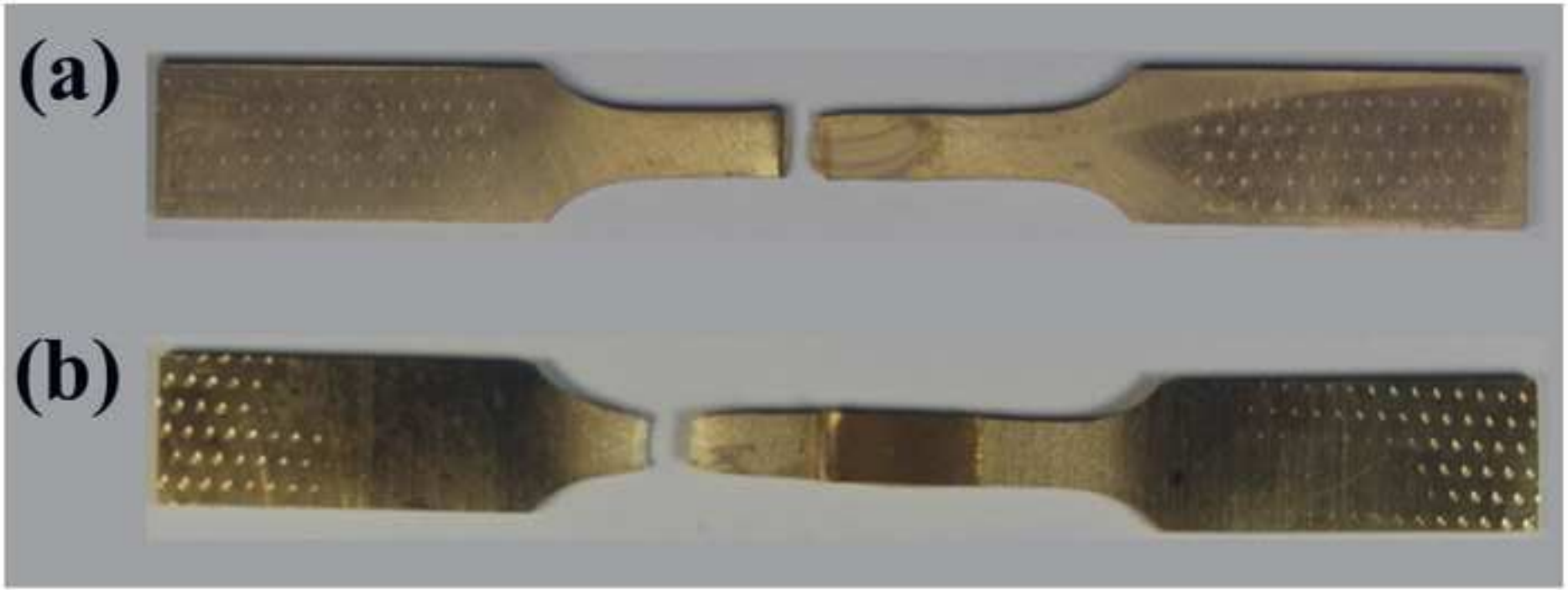

Figure 10

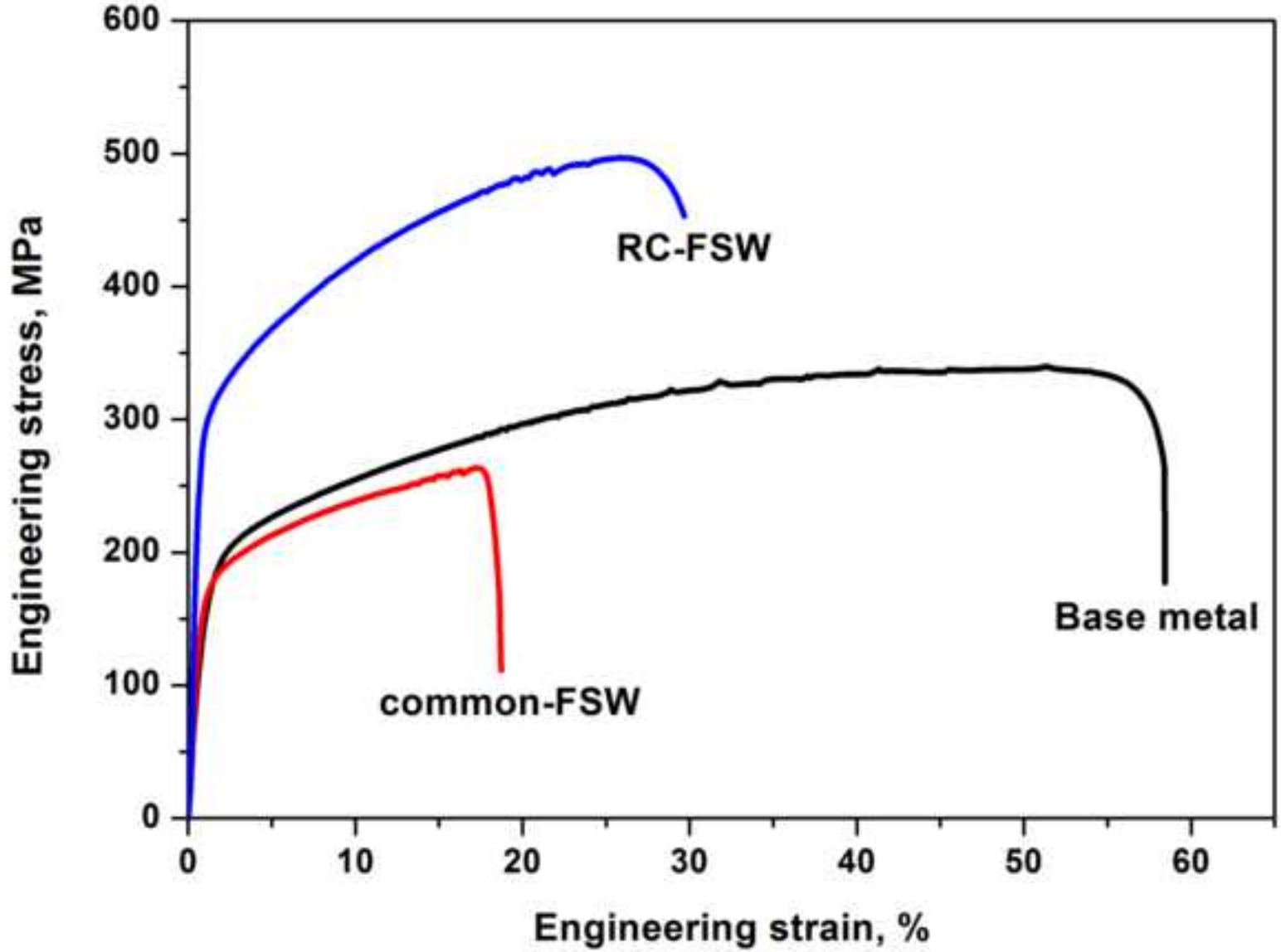
600
500
400
300
200
100
0
0
10
20
30
40
50
60
Engineering stress, MPa
Engineering strain, %
RC-FSW
common-FSW
Base metal